Organic–Inorganic Composite Nanocoatings with Superhydrophobicity, Good Transparency, and Thermal Stability

Qian Feng Xu,[†] Jian Nong Wang,[‡,*] and Kevin D. Sanderson[§]

[†]Shanghai Key Laboratory for Laser Processing and Materials Modification, School of Materials Science and Engineering, Shanghai Jiao Tong University, 800 Dong Chuan Road, Shanghai 200240, People's Republic of China, [‡]Shanghai Key Laboratory for Metallic Functional Materials, Key Laboratory for Advanced Civil Engineering Materials (Ministry of Education), School of Materials Science and Engineering, Tongji University, 1239 Siping Road, Shanghai 200092, People's Republic of China, and [§]Building Products, Research & Development, Pilkington Group Limited, Pilkington European Technical Centre, Hall Lane Lathom Ormskirk Lancashire L40 5UF, England

ABSTRACT Superhydrophobic, highly transparent, and stable organic–inorganic composite nanocoating is successfully prepared by a simple sol–gel dip-coating method. This method involves control of the aggregation of inorganic colloid particles by polymerization and ultrasonic vibration to create the desired micro/nanostructure in the coating. Superhydrophobicity and transparency of the coating can be controlled by adjusting the initial concentration of monomer and the size of aggregates in the sol–gel. Thus, superhydrophobicity and high transparency can be concurrently achieved in a single coating. The prepared coating also possesses good thermal stability. Its superhydrophobicity can be maintained from 20 to 90 °C.

KEYWORDS: superhydrophobicity · transparency · reversible aggregation · sol–gel · organic–inorganic composite coating

Superhydrophobic surfaces with a water contact angle (CA) larger than 150° and a sliding angle (SA) lower than 10° have recently attracted significant attention because of their unique water-repellency and self-cleaning properties and their potential applications ranging from small nonwetting micro/nanoelectronics to big self-cleaning building products.[1−10] In Nature, many plants and animals utilize superhydrophobic surfaces for special purposes.[11−13] Well-known examples include lotus leaves with self-cleaning properties and water striders that are able to walk and jump on water surface. A dual-scale structure has proven to be an essential feature in generating superhydrophobic coatings and especially important for obtaining low water sliding angles (SA).[14−20] Inspired by Nature, artificial superhydrophobic surfaces have been fabricated by using various techniques to control the roughness and structure of surfaces, such as colloidal self-assembly,[21,22] wet chemical etching,[23] inorganic or organic template,[24,25] electrospinning,[26,27] and phase separation.[28] However, many of the techniques involve multisteps or expensive reagent and special equipment, and some of the methods are only applicable to small surfaces. In addition, because superhydrophobicity requires very high surface roughness, which leads to extensive light scattering,[29−33] it is a technical challenge to achieve superhydrophobicity and transparency simultaneously by a single coating. As a result, the practical application of superhydrophobic coatings on optically transparent materials (such as solar cells and window glass) is limited.

In this study, we present a simple and inexpensive sol–gel dip-coating method that facilitates the fabrication of large-area superhydrophobic organic–inorganic composite nanocoatings. The surface structure, superhydrophobicity, and transparency of the coating can be controlled by adjusting the initial concentration of the monomer, and the surface free energy of the coating can be lowered by surface fluorination. The optimized coating shows not only an excellent superhydrophobicity but also a high transparency. Moreover, the coating possesses good thermal and chemical stabilities. The superhydrophobicity of the prepared coating remains unchanged after exposure to air for 1 year. The adhesion between the coating and the glass substrate is generated from the cross-linked chemical bonds and polarity groups in the polymers.

RESULTS AND DISCUSSION

Aggregation. The inorganic silica colloid particles prepared by the typical Stöber

*Address correspondence to jnwang@tongji.edu.cn.

Received for review November 8, 2009 and accepted March 08, 2010.

Published online March 19, 2010. 10.1021/nn901581j

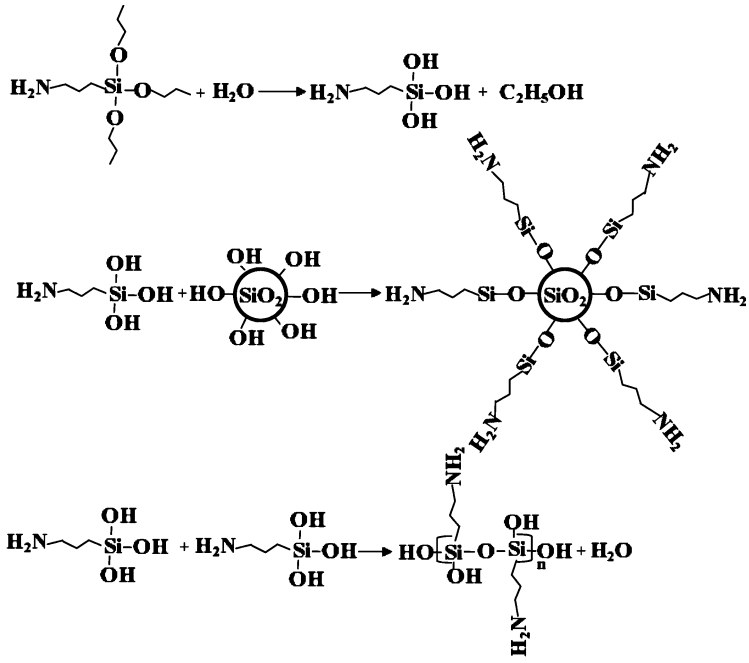

Figure 1. Schematics of the hydrolyzation of APS and the subsequent polycondensation between the hydrolyzed APS molecules and the silica colloid particles or between the hydrolyzed APS molecules.

method were monodisperse and had active hydroxyl groups on its surface.[34] γ-Aminopropyltriethoxysilane (APS) was selected as a reunion agent to aggregate the silica colloid particles because it has one amino and three ethoxy functional groups in its molecule. The possible chemical reactions are shown in Figure 1. When APS meets water contained in the silica sol, the ethoxy groups of APS hydrolyze immediately, generating 1−3 hydroxyl groups on each molecule. Then, dehydration or dealcohol polycondensation may occur between the hydrolyzed APS molecules and the hydroxyl groups on silica colloid particles or only between the hydrolyzed APS molecules. As a result, the silica colloid particles can be covered and aggregated by the formed poly-APS.

In this research, acetic acid was used as catalyst. It was found that the reaction temperature and the APS concentration were the two important parameters that could affect the hydrolyzation and polycondensation process. When the reaction temperature was set at 20 °C, even for the sols of high APS concentration, its viscosity and color nearly remained unchanged after stirring for more than 10 h. This result proves that at 20 °C the hydrolyzation and polycondensation speed of APS in the silica sol was very slow. When the reaction temperature was increased to 65 °C, the viscosity and color of the sols with a low APS concentration changed obviously with the stirring time. Particularly, for a high APS concentration, the sols could turn to a soupy or even semisolid state in only 15−30 min. The increase of viscosity was mainly due to the formation of poly-APS, and the color change may be due to the aggregation of colloid particles. With the special purpose of APS for aggregating the colloid particles, the reaction temperature was set at 60 °C.

TEM was used to detect the effect of APS on the aggregation of silica colloid particles. The TEM images are shown in Figure 2a−h. When a small amount of APS (0.12% in weight) was added into the sol, it can be seen from Figure 2a,b that a lot of small polymer particles formed in the sol, and every silica colloid particle was successfully covered by a thin layer of the formed polymer. The thickness of the polymer layer was 10−20 nm. Some of the covered silica colloid particles showed an obvious trend to aggregate with each other, though some of the covered silica colloid particles remained separate. When the concentration of APS was increased to 0.24%, it can be seen from Figure 2c,d that more polymer formed in the sol, and most of the silica colloid particles were connected by the polymer net. In Figure 2c, only several colloid particles existed separately. Comparing panels b and d of Figure 2, it can be found that the distance or the thickness of the mid polymer layer between the aggregated silica colloid particles became larger with the increase of APS addition. This observation indicates that hydrolyzed APS was inclined to polycondensate with the colloid particles as cores. When the APS concentration was increased to 0.36%, the sols turned to paste-like in 30 min. It can be seen from Figure 2e,f that a denser polymer net formed, and no separate silica colloid particles were detected. In another word, all of the silica colloid particles were arrested by the polymer net. When the concentration of APS was increased to 0.6%, the sols turned to into a semisolid state in only 15 min. The microstructure of the gel is shown in Figure 2g,h. It can be seen that a polymer net with a strong three-dimensional (3-D) cross-linking structure formed, and the silica colloid particles distributed in the polymer net uniformly and densely.

Re-dispersion. After the step of aggregation, all of the sol−gels were re-dispersed by a simple method of ultrasonic vibration in ice water for 20 min. It was found that the paste-like or semisolid gels turned into transparent sols with good fluidity again after the simple ultrasonic vibration, and the re-dispersed sols can be stored stably for several days at room temperature (~25 °C).

The optical images of a sol without APS addition and a re-dispersed sol with 0.36% APS addition are shown in Figure 3a. It can be seen that the transparency of the re-dispersed sol is much lower than the sol

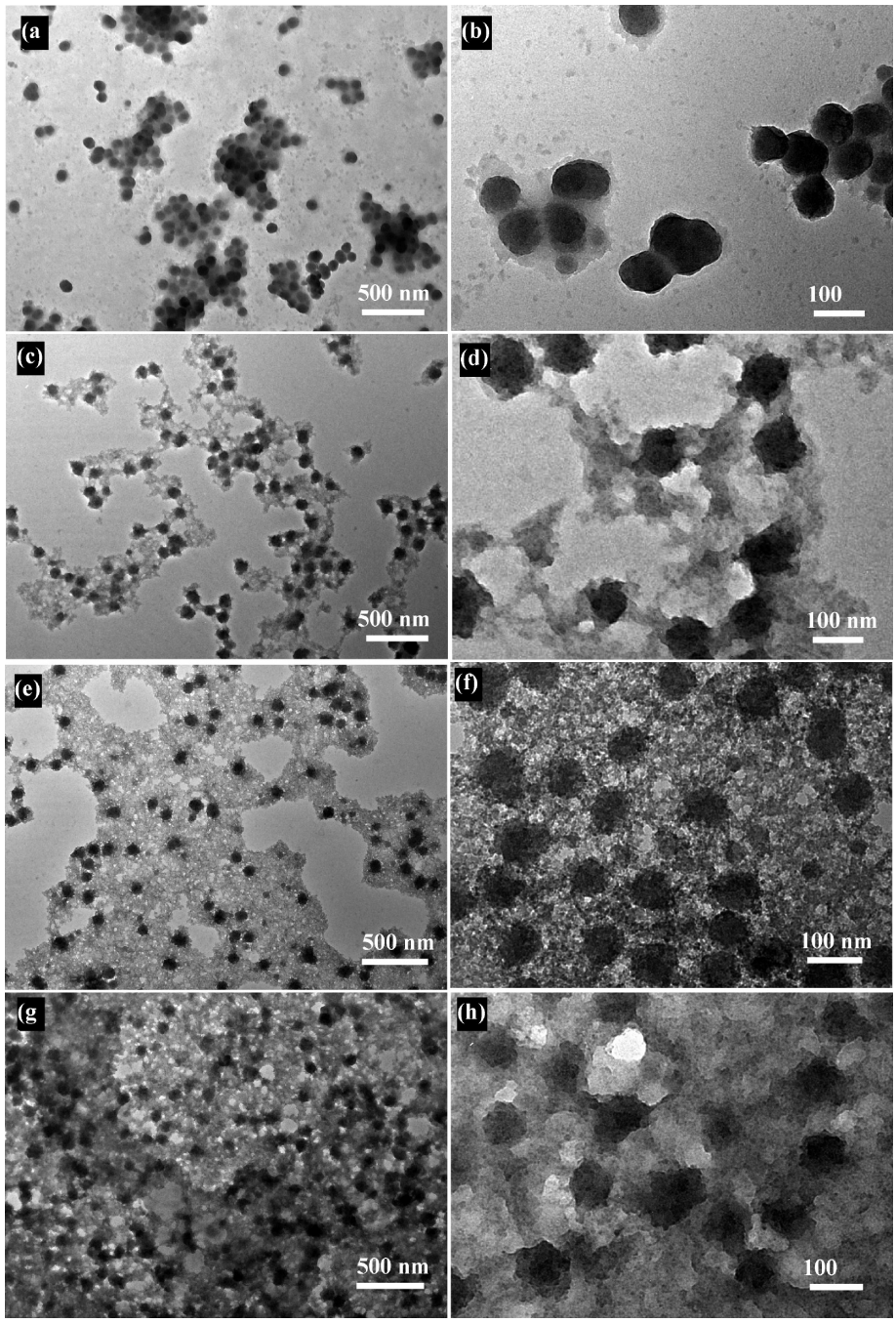

Figure 2. TEM images of sol−gels with different APS additions: (a,b) 0.12%, (c,d) 0.24%, (e,f) 0.36%, and (g,h) 0.6%. Panels b, d, g, and h are the higher magnifications of panels a, c, e, and f, respectively.

without APS addition. The microstructure of the re-dispersed sols was examined by TEM, and the results are shown in Figure 3b,c. Comparing panels e and f of Figure 2, it can be seen that many parts of the polymer net were torn open by the ultrasonic vibration, forming some small colloid aggregates. This may be the main reason why the re-dispersed sols regained good fluidity. This result indicates that there were reversible aggregations taking place in the sol. Because the Si−O−Si chemical bond energy is very high and the intensity of the ultrasonic vibration used in this research was only 0.75 W cm^{-2}, much lower than the high-intensity ultrasonic probes (50−500 W cm^{-2}) used for biological cell disruption, it was almost impossible to re-open Si−O−Si bonds by this simple ultrasonic vibration. The torn part of the polymer net must be the weakest part in the polymer net aggregated only by long-range forces.[35] The aminopropyl group in poly-APS had two effects in the aggregation and re-dispersion process. On one hand, it could increase the attractive force between polymer molecules by generating hydrogen bonds or other long-range forces and is thus useful for the aggregation of colloid particles. On the other hand, the aminopropyl group has a steric ef-

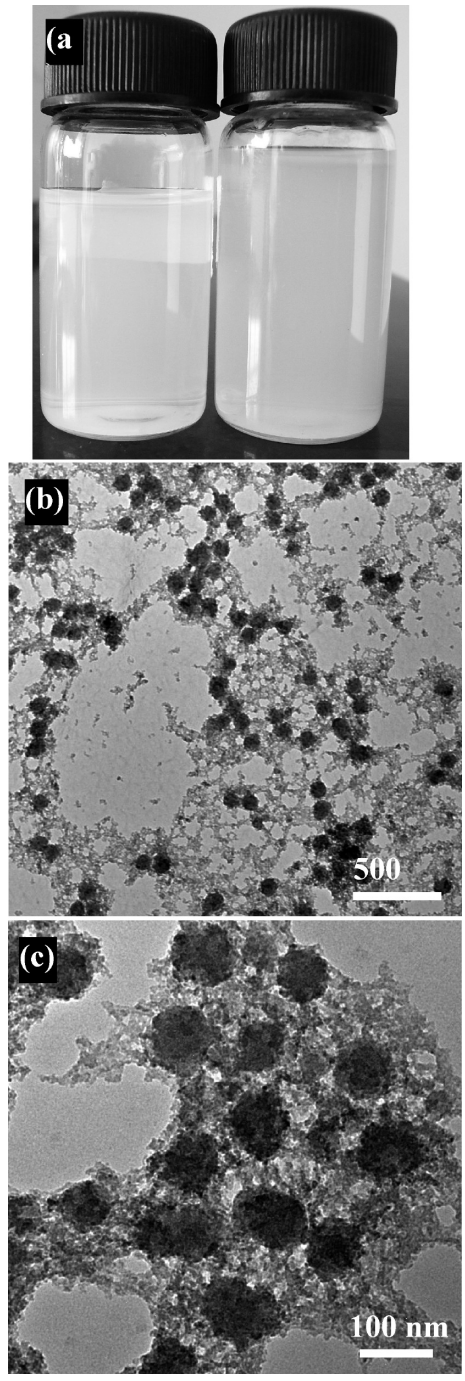

Figure 3. (a) Optical images of sols without (left) or with (right) 0.36% APS addition after reaction and ultrasonic vibration. (b,c) TEM images of a sol containing 0.36% APS after ultrasonic vibration. (c) High magnification of (b).

fect in forming Si−O−Si chemical bonds between hydroxyl groups of poly-APS. As a result, some poly-APS molecules were aggregated by long-range forces without Si−O−Si chemical bonds. During the ultrasonic vibration, these weak aggregations could be reopened. The silica colloid particles in the re-dispersed sol could not be dispersed thoroughly, and the main existing forms were small aggregates composed of silica colloid particles and polymers. This may be the reason that the re-dispersed sols had a much lower transparency than the sols with no APS addition.

Surface Structure and Superhydrophobicity. The re-dispersed sols were used to construct micro/nanostructures on glass substrates by a dip-coating method. AFM was used to examine the surface structures of the coatings, and the result is shown in Figure 4. For the coating prepared from sols containing 0.12% APS, it can be seen from Figure 4a that only less than half of the surface of the glass substrate was covered by silica colloid particles, and from Figure 4b, it can be seen that there were several separated bumps on the surface. While for the coating prepared from sols containing 0.36% APS (Figure 4c) nearly the entire surface of the glass substrate was covered by silica colloid particles, the silica colloid particles on the surface constructed a porous structure instead of forming a dense hexagonal arrangement. From Figure 4d, it can be seen that the surface structure was composed of nanoparticles and bumps. The bumps in Figure 4b,d were formed by the deposition of silica colloid aggregates during the repeating dip-coating process, and the height of the bumps was strongly affected by the size of the aggregates. Because the sols of high APS concentration had a higher viscosity, more sol was carried by the glass substrate surface in each withdrawing process. As a result, the surface was covered fully by silica colloid particles for sols with a high APS concentration. Examination on many regions at a much lower magnification than that shown in Figure 4 revealed that the coating prepared by this method was homogeneous.

The water-repellent properties of the coatings after perfluoroalkylsilane (FAS) modification were researched by measuring the static CA and dynamic SA of a water droplet of 4.0 μL. The static CAs were 140 ± 1, 148 ± 1, 155 ± 1, 160 ± 1, and 165 ± 1° for the APS concentration of 0.12, 0.24, 0.36, 0.48, and 0.6%, respectively. It is obvious that the static CA increases with the APS concentration. The typical optical images of water droplets on different surfaces are shown in Figure 5a−d. When the APS concentration was lower than 0.36%, the coatings did not show superhydrophobicity. The static CAs on the coatings were less than 150°, and the water droplet could not slide easily. When the APS concentration was increased to be equal to or higher than 0.36%, the static CAs of the water droplet on all of the coatings were larger than 155°. The water droplets became very unstable on these surfaces, and a gentle vibration could make the water droplets roll away. The rolling process of a water droplet on a slightly tilted (less than 2°) superhydrophobic surface is shown in Figure 5e,f. It can be seen that the water droplets remained as a ball during the rolling process, and thus such a superhydrophobic surface can be used for self-cleaning.

It has been found that when the chemical composition is kept the same the surface structure is the main factor affecting the static CA. Wenzel's[36] and

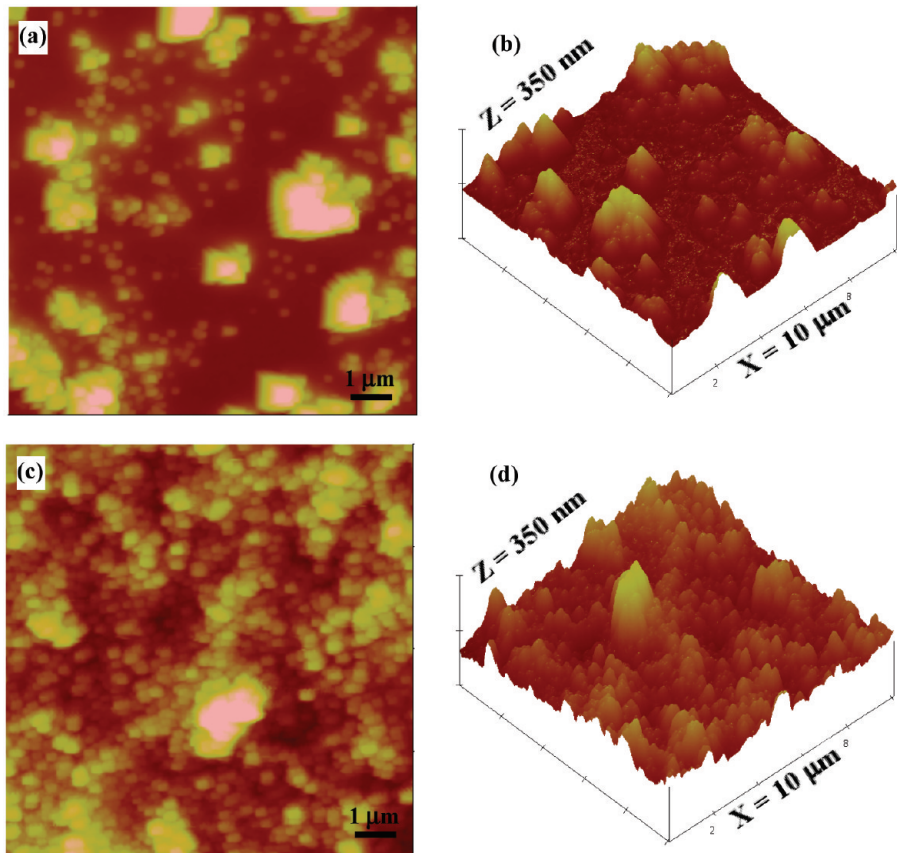

Figure 4. AFM images of a surface dip-coated from re-dispersed sols containing different APS concentrations: (a,b) 0.12% and (c,d) 0.36%; (a,c) 2-D images and (b,d) 3-D images.

Cassie−Baxter's[37] models are two typical empirical models often used for explaining the relationship between the superhydrophobicity and the surface structure. In Wenzel's model, the air trapped in the rough surface can be piled out by water, and the substrate can be wetted.[14] Thus, the adhesion between the water droplet and substrate is large. However, in Cassie's model, the rough surface is not wetted and can trap air in pores. As a result, the adhesion between the water droplet and substrate is weak and even can be neglected. For the coatings prepared from sols containing APS lower than 0.24%, the surface is composed of separate bumps. The water droplet on this coating is consistent with the case of Wenzel's model. That is, the air trapped on the surface is piled out by water, and the surface is wetted. As a result, the CA is not high, the adhesion force between the water droplet and substrate is large, and the water droplet is difficult to slide. For the coatings prepared from sols containing APS equal to or higher than 0.36%, the surface is composed of nanoparticles and bumps, with the nanoparticles being between the bumps. When a water droplet is placed on this coating, these nanoparticles can discontinue the contact area between the water and the surface, and the state of the water droplet may turn into the case of Cassie's model. Consequently, a higher CA was observed, and the adhesion force between the water droplet and the substrate was very small and even could be neglected.

Transparency. While increasing roughness is favorable for superhydrophobicity, such increase is detrimental to transparency as light scattering is severe on a rough surface. It is reported that the surface roughness should be controlled to be less than 100 nm in order to minimize light scattering and achieve good transparency. Otherwise, the coating would become opaque or translucent.[10] The optical images of glass substrates with superhydrophobic coatings prepared from sols of different APS concentrations are shown in Figure 6a−d. The water droplets on these superhydrophobic coatings had high CAs and looked like transparent balls. The transparency of the coated glass could be estimated from the clarity of the letters underneath the glass. The clarity of the letters decreased with the increase of APS concentration. For the glass substrates coated from sols containing 0.36 and 0.48% APS, the letters underneath the glass substrates were very clear. While for the glass substrate coated from sols containing much more APS, the letters became unclear, or even blurred. The transmittance spectra of the coated glasses in the UV−vis wavelength range are shown in Figure 6e. When the APS concentration was as low as 0.12%, the transmittance spectrum of the coated glass was very close to but lower than the transmittance spectrum of the un-

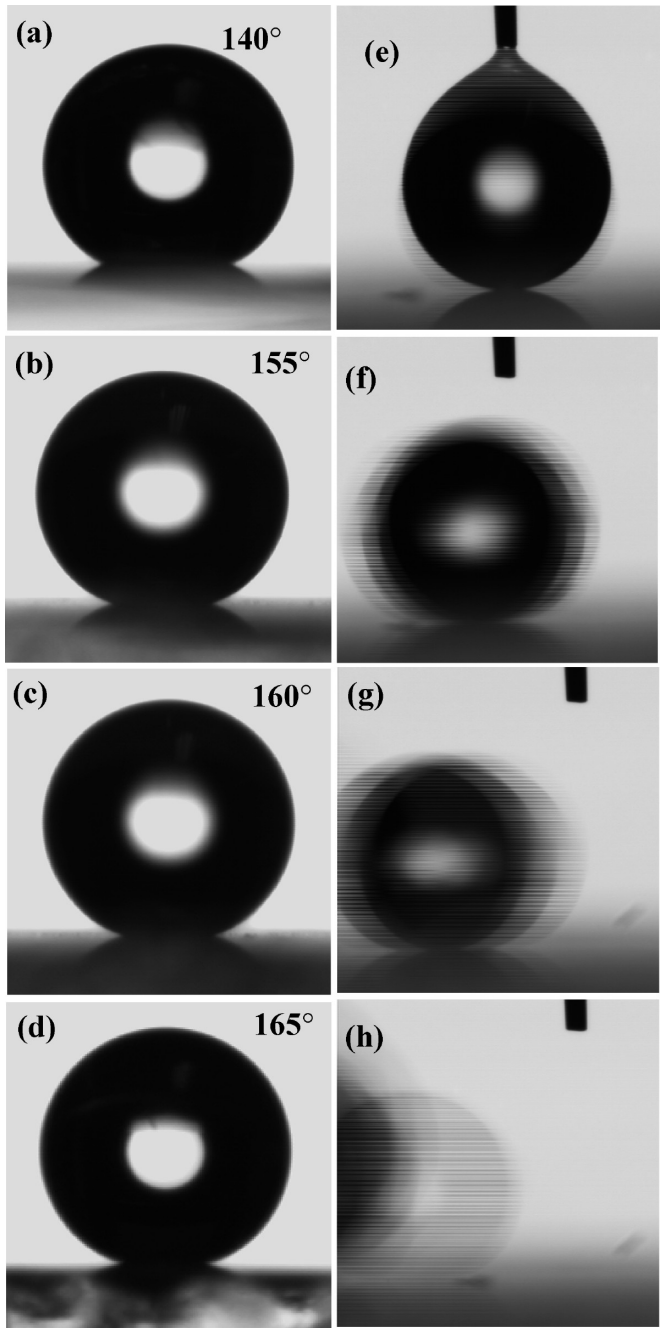

Figure 5. Optical images of water droplets on surfaces dip-coated from sols containing (a) 0.12% APS, CA = 140°, (b) 0.36% APS, CA = 155°, (c) 0.48% APS, CA = 160°, (d) 0.6% APS, CA = 165°, and the rolling process of a water droplet on the surface coated from sols containing 0.36% APS and tilted by an angle less than 2°.

coated glass. While when the APS concentration was increased to 0.72%, the transmittance of the coated glass decreased to 60%, and the coated glass became translucent. It became difficult to see through this translucent glass from a shot distance by the naked eye. In contrast to superhydrophobicity, the transmittance decreased gradually with the increase of APS concentration. The roughness of the surface was determined by the surface structure, and the bumps in the surface were strongly affected by the size of the aggregates. The size of the bumps in the surface became larger as well as the size of the aggregates with the increase of APS concentration. As a result, the light scattering increased, and thus a lower transparency was observed. This result demonstrates that it is a practical way to control the transparency and superhydrophobicity of the coatings by adjusting the APS concentration. In particular, when the APS concentration was 0.36%, the coating showed both superhydrophobicity and good transparency, the static CA was as high as 155°, and the highest transmittance was 88%.

Chemical Composition and Thermal Stability. The surface free energy of the coating was lowered by a simple chemical modification of FAS. The XPS spectrum results are shown in Figure 6f. Before the FAS modification, the surface chemical elements were mainly composed of Si, O, C, and N, and it could be deduced that the surface chemical groups were OH and NH_2. Such a surface was very hydrophilic. However, after the FAS modification, a strong fluorine peak at 686.5 eV is observed, and it can be seen that the intensity of Si, O, and N peaks decreased after the FAS modification. The atomic ratios of the surface elements before and after the FAS modification were calculated by curve area integrals. The atomic ratios of Si, O, and N decreased from 24.5, 40.2, and 4.7% to 14.0, 23.46, and 3.17%, respectively, although the atomic ratio of C remained nearly unchanged. These results prove that the coating was successfully covered by FAS. The long chain of FAS was composed of CH_2, CF_2, and CF_3 groups with extremely low free energies, and it could cap the hydrophilic groups such as NH_2 and OH spontaneously. As a result, the surface turned very hydrophobic after the FAS modification. The change of the surface chemical groups before and after FAS modification is schematically shown in Figure 7a,b.

The thermal stability of the prepared superhydrophobic and transparent coating was tested by measuring the static CAs at different temperatures. The temperature of the glass substrates was controlled by a hot plate. The water droplet was placed on the surface for 3 min to make the water temperature the same as that of the glass surface, and then the contact angle was measured. The result is shown in Figure 7c. The static CA was nearly unchanged, with the temperature increased from 20 to 90 °C, showing a good thermal stability of the coating.

CONCLUSIONS

In summary, an organic−inorganic composite coating with superhydrophobicity, good transparency, and thermal stability was successfully fabricated by a simple sol−gel dip-coating method based on partially reversible aggregation of silica colloid particles. The silica colloid particles aggregated by poly-APS can be redispersed partially by ultrasonic vibration, forming a

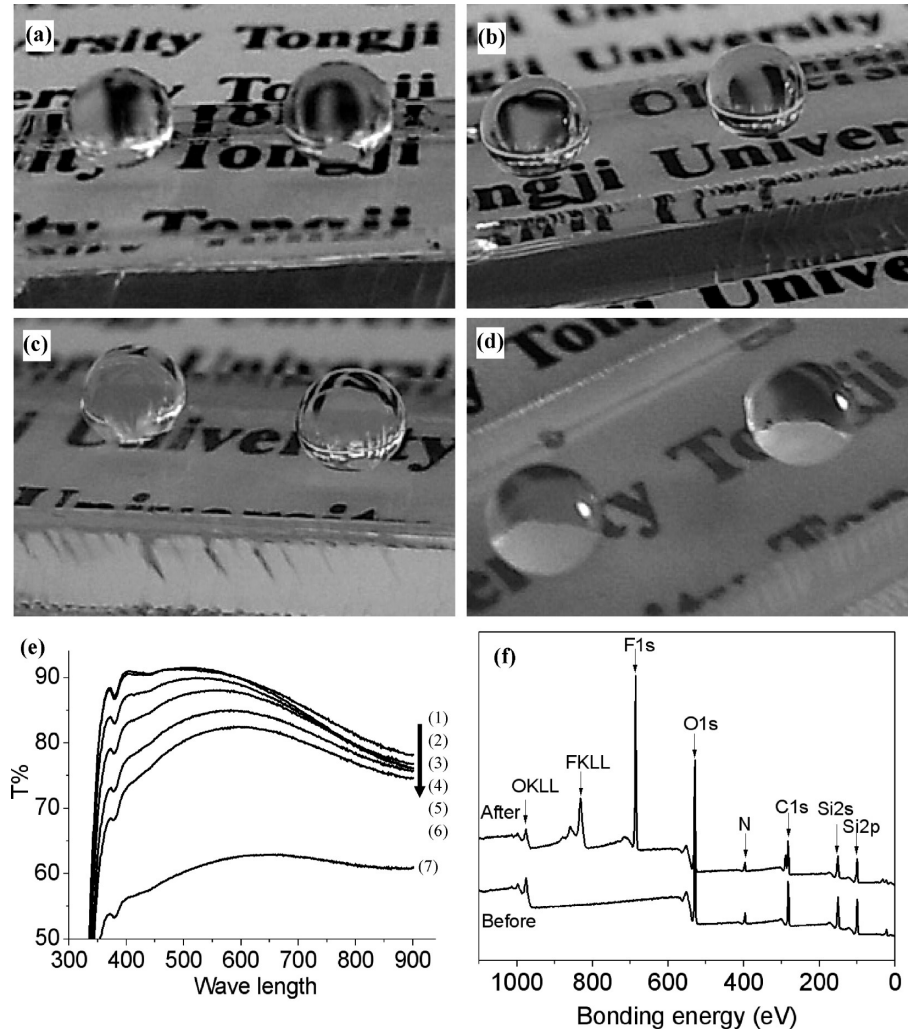

Figure 6. Optical images of glass substrates with superhydrophobic coatings from sols containing (a) 0.36% APS, (b) 0.48% APS, (c) 0.6% APS, and (d) 0.72% APS; transmittance results of different glass substrates (e) [(1) not coated, (2−7) dip-coated from sols containing 0.12, 0.24, 0.36, 0.48, 0.6, and 0.72% APS], and XPS spectra of the coatings before and after FAS modification (f).

lot of small aggregates. These aggregates are consequently assembled onto the glass substrate by dip-coating. It is shown that the surface structure, superhydrophobicity, and transparency can be controlled by adjusting the APS concentration. When the concentration of APS was 0.36%, the static CA of a 4 μL water droplet on the coating is as high as 155°, and SA is lower than 2°. Additionally, the highest transmittance of the coated glass can reach 88%. The prepared coating also possesses good thermal stability. Its superhydrophobicity can be maintained from 20 to 90 °C. The present method has advantages for easy simultaneous achievement of superhydrophobicity and high transparency, as well as being suitable for large-scale coating.

EXPERIMENTAL SECTION

Preparation of Sols. At first, a monodisperse silica sol was prepared by a typical Stöber method using ammonia as catalyst. Three milliliters of tetraethylorthosilicate (TEOS) was added into 45 mL of ethanol, and 3 mL of ammonia (25 wt %) was added into the solution. The mixed solution was stirred at 50 °C for 1 h. After this, the color of the sol turned a transparent blue, and nearly all TEOS was reacted in forming silica colloid particles. The average diameter of the colloid particles was about 60 nm. In order to improve the stability of the prepared silica sol, NH_3 was removed by stirring the sol in an open Petri dish in a ventilating cabinet. The solid concentration of the target silica sol was 2.5%.

γ-Aminopropyltriethoxysilane (APS) was then used to aggregate the silica colloid particles in the prepared sols. Different amounts of APS were added dropwise from a syringe, and a certain amount of acetic acid was used to adjust the pH value to 3. The mixed sol was stirred at 20−65 °C for 15−60 min. After this, all of the sol−gels were cooled in ice water immediately and redispersed by ultrasonic vibration for 20 min to open the reversible aggregation between the colloid particles.

Dip-Coating and Surface Fluorination. Transparent flat-glass slices of 2 × 5 cm were used as substrates. All substrates were cleaned with a H_2SO_4/H_2O_2 (50/50 wt %) solution for 1 h and ultrasonicated in acetone for 10 min, and then rinsed by a large amount of distilled water before coating. The cleaned substrate was immersed into the sol for 5 min before the first dip-coating and 5 s

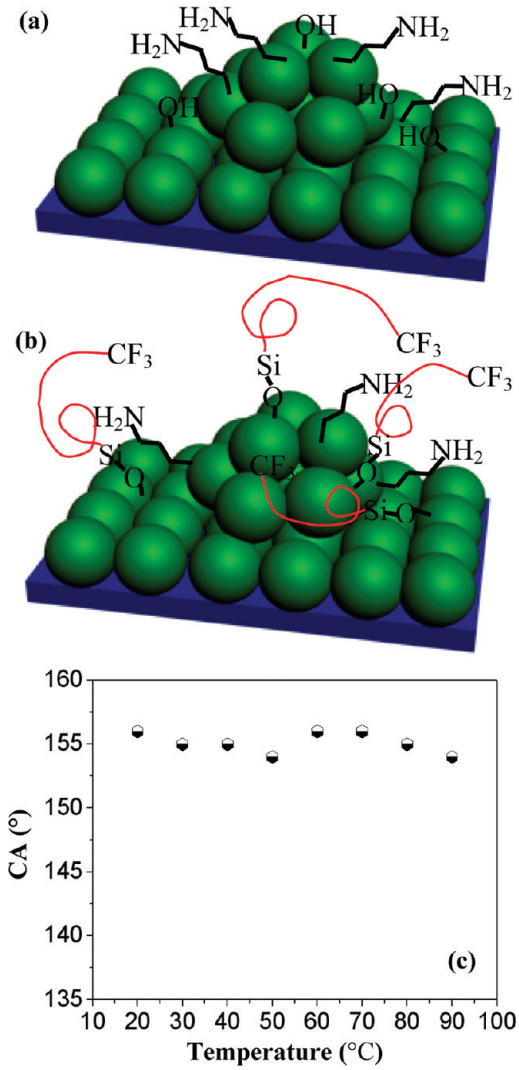

Figure 7. Schematics of the chemical groups on the surfaces before (a) and after (b) FAS modification, and the static contact angles (CA) of a water droplet on the superhydrophobic surface at different temperatures.

before the subsequent dip-coating. The withdrawing speed was kept at 0.45 mm s^{-1}. After each coating, the substrate was dried at room temperature (~25 °C) for 3 min, and this step was repeated five times. The coated glass substrates were heated at 120 °C for 30 min to remove the residual solvent and solidify the coatings, and then a simple surface fluorination procedure was conducted to lower the surface free energy by chemically grafting a layer of perfluoroalkylsilane (FAS) on the surface. FAS solution was prepared by adding 1:100 (vol %) FAS and triplicate water into methanol. The coated glass substrates were put into a sealed vessel containing 0.3 mL of FAS solution. The distance between the glass substrate and the solution was 55 mm. The vessel was kept at 150 °C for 3 h to cover the coatings by a layer of FAS.

Characterization. The microstructure and aggregation of sol−gels were examined by transmission electron microscopy (TEM) (JEM-2010, INCA OXFORD). The sol−gels were diluted by ethanol to prepare TEM samples, and the dilution was manipulated gently without violent stirring or vibration to avoid the possible damage to the colloidal aggregation. The roughness and morphology of the surfaces were characterized by atomic force microscopy (AFM) (Multimode Nanoscope IIIa, USA). The static CA and dynamic SA were measured by a contact angle meter (OCA20, Germany). Several microliters of pure water (18.2 MΩ · cm in resistivity) were placed slowly and carefully onto the surfaces at ambient atmosphere, and the static CA was measured at different positions at least five times. X-ray photoelectron spectroscopy (XPS) (Monochromated Al Kα, Kratos Axis Ultra DLD) was used to detect the chemical compositions of the coating surface. The transmittance spectra of prepared SH coatings were determined by a UV−vis spectrophotometer (Evolution 300, USA).

Acknowledgment. Financial support from Pilkington Group Limited is appreciated.

REFERENCES AND NOTES

1. Lafuma, A.; Quere, D. Superhydrophobic States. *Nat. Mater.* **2003**, *2*, 457–460.
2. Mumm, F.; van Helvoort, A. T. J.; Sikorski, P. Easy Route to Superhydrophobic Copper-Based Wire-Guided Droplet Microfluidic Systems. *ACS Nano* **2009**, *3*, 2647–2652.
3. Koch, K.; Bhushan, B.; Barthlott, W. Diversity of Structure, Morphology and Wetting of Plant Surfaces. *Soft Matter* **2008**, *4*, 1943–1963.
4. Zhai, L.; Cebeci, F. C.; Cohen, R. E.; Rubner, M. F. Stable Superhydrophobic Coatings from Polyelectrolyte Multilayers. *Nano Lett.* **2004**, *4*, 1349–1353.
5. Xu, Q. F.; Wang, J. N. A Superhydrophobic Coating on Aluminium Foil with an Anti-corrosive Property. *New J. Chem.* **2009**, *33*, 734–738.
6. Li, X. M.; Reinhoudt, D.; Crego-Calama, M. What do We Need for a Superhydrophobic Surface? A Review on the Recent Progress in the Preparation of Superhydrophobic Surfaces. *Chem. Soc. Rev.* **2007**, *36*, 1350–1368.
7. Tuteja, A.; Choi, W.; Ma, M. L.; Mabry, J. M.; Mazzella, S. A.; Rutledge, G. C.; McKinley, G. H.; Cohen, R. E. Designing Superoleophobic Surfaces. *Science* **2007**, *318*, 1618–1622.
8. Gao, L. C.; McCarthy, T. J. A Perfectly Hydrophobic Surface (θ_A/θ_R = 180°/180°). *J. Am. Chem. Soc.* **2006**, *128*, 9052–9053.
9. Zhu, Y.; Zhang, J. C.; Zheng, Y. M.; Huang, Z. B.; Feng, L.; Jiang, L. Stable, Superhydrophobic, and Conductive Polyanilind/Polystyrene Films for Corrosive Environments. *Adv. Funct. Mater.* **2006**, *16*, 568–574.
10. Nakajima, A.; Fujishima, A.; Hashimoto, K.; Watanabe, T. Preparation of Transparent Superhydrophobic Boehmite and Silica Films by Sublimation of Aluminum Acetylacetonate. *Adv. Mater.* **1999**, *11*, 1365–1368.
11. Barthlott, W.; Neinhuis, C. Purity of the Sacred Lotus, or Escape from Contamination in Biological Surfaces. *Planta* **1997**, *202*, 1–8.
12. Cheng, Y.; Rodak, D. E. Is the Lotus Leaf Superhydrophobic? *Appl. Phys. Lett.* **2005**, *86*, 144101.
13. Gao, X.; Jiang, L. Water-Repellent Legs of Water Striders. *Nature* **2004**, *432*, 36.
14. Darmanin, T.; Guittard, F. Super Oil-Repellent Surfaces from Conductive Polymers. *J. Mater. Chem.* **2009**, *19*, 7130–7136.
15. Chen, M. H.; Hsu, T. H.; Chuang, Y. J.; Tseng, F. G. Dual Hierarchical Biomimic Superhydrophobic Surface with Three Energy States. *Appl. Phys. Lett.* **2009**, *95*, 023702.
16. Tuteja, A.; Choi, W. J.; McKinley, G. H.; Cohen, R. E.; Rubner, M. F. Design Parameters for Superhydrophobicity and Superoleophobicity. *MRS Bull.* **2008**, *33*, 752.
17. Quere, D. Wetting and Roughness. *Annu. Rev. Mater. Res.* **2008**, *38*, 71–99.
18. Patankar, N. A. Transition between Superhydrophobic States on Rough Surfaces. *Langmuir* **2004**, *20*, 7097–7102.
19. Gao, L. C.; McCarthy, T. J. The "Lotus Effect" Explained: Two Reasons Why Two Length Scales of Topography Are Important. *Langmuir* **2006**, *22*, 2966–1967.
20. Xu, Q. F.; Wang, J. N.; Smith, I. H.; Sanderson, K. D. Directing the Transportation of a Water Droplet on a Patterned Superhydrophobic Surface. *Appl. Phys. Lett.* **2008**, *93*, 233112.
21. Zhang, G.; Wang, D. Y.; Gu, Z. Z.; Mohwald, H. Fabrication of Superhydrophobic Surfaces from Binary Colloidal Assembly. *Langmuir* **2005**, *21*, 9143–9148.

22. Hong, J.; Bae, W. K.; Lee, H.; Oh, S.; Char, K.; Caruso, F.; Cho, J. Tunable Superhydrophobic and Optical Properties of Colloidal Films Coated with Block-Copolymer-Micelles/Micelle-Multilayers. *Adv. Mater.* **2007**, *19*, 4364.
23. Xiu, Y.; Zhu, L.; Hess, D. W.; Wong, C. P. Hierarchical Silicon Etched Structures for Controlled Hydrophobicity/Superhydrophobicity. *Nano Lett.* **2007**, *7*, 3388–3393.
24. Neto, C.; Joseph, K. R.; Brant, W. R. On the Superhydrophobic Properties of Nickel Nanocarpets. *Phys. Chem. Chem. Phys.* **2009**, *11*, 9537–9544.
25. Xu, Q. F.; Wang, J. N.; Smith, I. H.; Sanderson, K. D. Superhydrophobic and Transparent Coatings Based on Removable Polymeric Spheres. *J. Mater. Chem.* **2009**, *19*, 655–660.
26. Valtola, L.; Koponen, A.; Karesoja, M.; Hietala, S.; Laukkanen, A.; Tenhu, H.; Denifl, P. Tailored Surface Properties of Semi-fluorinated Block Copolymers by Electrospinning. *Polymer* **2009**, *50*, 3103–3110.
27. Ma, M.; Hill, R. H.; Lowery, J. L.; Fridrikh, S. V.; Rutledge, G. C. Electrospun Poly(styrene-*co*-dimethylsiloxane) Block Copolymer Fibers Exhibiting Microphase Separation and Superhydrophobicity. *Langmuir* **2005**, *21*, 5549–5554.
28. Zhao, N.; Xie, Q. D.; Weng, L. H.; Wang, S. Q.; Zhang, X. Y.; Xu, J. Superhydrophobic Surface from Vapor-Induced Phase Separation of Copolymer Micellar Solution. *Macromolecules* **2005**, *38*, 8996–8999.
29. Li, Y.; Liu, F.; Sun, J. Q. A Facile Layer-by-layer Deposition Process for the Fabrication of Highly Transparent Superhydrophobic Coatings. *Chem. Commun.* **2009**, *19*, 2730–2732.
30. Lin, L. Y.; Kim, H. J.; Kim, D. E. Wetting Characteristics of ZnO Smooth Film and Nanowire Structure with and without OTS Coating. *Appl. Surf. Sci.* **2008**, *254*, 7370–7376.
31. Bravo, J.; Zhai, L.; Wu, Z.; Cohen, R. E.; Rubner, M. F. Transparent Superhydrophobic Films Based on Silica Nanoparticles. *Langmuir* **2007**, *23*, 7293–7298.
32. Artus, G. R. J.; Jung, S.; Zimmermann, J.; Gautschi, H.; Marquardt, K.; Seeger, S. Silicone Nanofilaments and Their Application as Superhydrophobic Coatings. *Adv. Mater.* **2006**, *18*, 2758–2762.
33. Shang, H. M.; Wang, Y.; Limmer, S. J.; Chou, T. P.; Takahashi, K.; Cao, G. Z. Optically Transparent Superbydrophohic Sillca-Based films. *Thin Solid Films* **2005**, *472*, 37.
34. Bourgeat-Lami, E.; Lang, J. Encapsulation of Inorganic Particles by Dispersion Polymerization in Polar Media - 1. Silica Nanoparticles Encapsulated by Polystyrene. *J. Colloid Interface Sci.* **1998**, *197*, 293–308.
35. Suslick, K. S.; Price, G. J. Applications of Ultrasound to Materials Chemistry. *Annu. Rev. Mater. Sci.* **1999**, *29*, 295–326.
36. Wenzel, R. N. Resistance of Solid Surfaces to Wetting by Water. *Ind. Eng. Chem.* **1936**, *28*, 988–994.
37. Cassie, A. B. D.; Baxter, S. Wettability of Porous Surfaces. *Trans. Faraday Soc.* **1944**, *40*, 546–551.